A multiple-resonator approach for broadband light absorption in a single layer of nanostructured graphene

Soongyu Yi,[1] Ming Zhou,[1] Xi Shi,[2] Qiaoqiang Gan,[3] Jian Zi,[2,4] and Zongfu Yu[1,*]

[1]*Department of Electrical and Computer Engineering, University of Wisconsin, Madison, Wisconsin 53705, USA*
[2]*Department of Physics, Key Laboratory of Micro- and Nano-Photonic Structures (MOE), and State Key Laboratory of Surface Physics, Fudan University, Shanghai 200433, China*
[3]*Department of Electrical and Computer Engineering, University of Buffalo, Buffalo, New York 14260, USA*
[4]*Collaborative Innovation Center of Advanced Microstructures, Nanjing University, Nanjing 210093, China*
[*]*zyu54@wisc.edu*

Abstract: The interaction between two-dimensional (2D) materials and light is rather weak due to their ultrathin thickness. In order for these emerging 2D materials to achieve performances that are comparable to those of conventional optoelectronic devices, the light-material interaction must be significantly enhanced. An effective way to enhance the interaction is to use optical resonances. Efficient light absorption has been demonstrated in a single layer of graphene based on a variety of resonators. However, the bandwidth of the absorption enhancement is always narrow, which limits its application for optoelectronic devices. In order to broaden the enhancement of light-material interaction, here we propose a multiple-resonator approach based on nanostructured graphene. These nanostructures having different geometry support resonances at different frequencies. Owing to their deep subwavelength sizes, graphene resonators can be closely packed in space, resulting in a high optical density of states, which enables the broadband light absorption.

OCIS codes: (050.6624) Subwavelength structures; (310.3915) Metallic, opaque, and absorbing coatings.

References and links

1. K. S. Novoselov, A. K. Geim, S. V. Morozov, D. Jiang, Y. Zhang, S. V. Dubonos, I. V. Grigorieva, and A. A. Firsov, "Electric Field Effect in Atomically Thin Carbon Films," Science **306**(5696), 666–669 (2004).
2. K. I. Bolotin, K. J. Sikes, Z. Jiang, M. Klima, G. Fudenberg, J. Hone, P. Kim, and H. L. Stormer, "Ultrahigh electron mobility in suspended graphene," Solid State Commun. **146**(9-10), 351–355 (2008).
3. F. Bonaccorso, Z. Sun, T. Hasan, and A. C. Ferrari, "Graphene photonics and optoelectronics," Nat. Photonics **4**(9), 611–622 (2010).
4. K. F. Mak, M. Y. Sfeir, Y. Wu, C. H. Lui, J. A. Misewich, and T. F. Heinz, "Measurement of the Optical Conductivity of Graphene," Phys. Rev. Lett. **101**(19), 196405 (2008).
5. M. Furchi, A. Urich, A. Pospischil, G. Lilley, K. Unterrainer, H. Detz, P. Klang, A. M. Andrews, W. Schrenk, G. Strasser, and T. Mueller, "Microcavity-Integrated Graphene Photodetector," Nano Lett. **12**(6), 2773–2777 (2012).
6. J. R. Piper and S. Fan, "Total Absorption in a Graphene Monolayer in the Optical Regime by Critical Coupling with a Photonic Crystal Guided Resonance," ACS Photonics **1**(4), 347–353 (2014).
7. Y. Liu, A. Chadha, D. Zhao, J. R. Piper, Y. Jia, Y. Shuai, L. Menon, H. Yang, Z. Ma, S. Fan, F. Xia, and W. Zhou, "Approaching total absorption at near infrared in a large area monolayer graphene by critical coupling," Appl. Phys. Lett. **105**(18), 181105 (2014).
8. F. H. L. Koppens, D. E. Chang, and F. J. García de Abajo, "Graphene Plasmonics: A Platform for Strong Light-Matter Interactions," Nano Lett. **11**(8), 3370–3377 (2011).
9. S. Zhang, D. A. Genov, Y. Wang, M. Liu, and X. Zhang, "Plasmon-Induced Transparency in Metamaterials," Phys. Rev. Lett. **101**(4), 047401 (2008).
10. H. Yan, X. Li, B. Chandra, G. Tulevski, Y. Wu, M. Freitag, W. Zhu, P. Avouris, and F. Xia, "Tunable infrared plasmonic devices using graphene/insulator stacks," Nat. Nanotechnol. **7**(5), 330–334 (2012).
11. S. Thongrattanasiri, F. H. Koppens, and F. J. García de Abajo, "Complete Optical Absorption in Periodically Patterned Graphene," Phys. Rev. Lett. **108**(4), 047401 (2012).

#234896 - $15.00 USD Received 18 Feb 2015; revised 6 Apr 2015; accepted 8 Apr 2015; published 10 Apr 2015

12. Z. Yu, A. Raman, and S. Fan, "Fundamental limit of nanophotonic light trapping in solar cells," Proc. Natl. Acad. Sci. U.S.A. **107**(41), 17491–17496 (2010).
13. D. M. Callahan, J. N. Munday, and H. A. Atwater, "Solar Cell Light Trapping beyond the Ray Optic Limit," Nano Lett. **12**(1), 214–218 (2012).
14. K. Aydin, V. E. Ferry, R. M. Briggs, and H. A. Atwater, "Broadband polarization-independent resonant light absorption using ultrathin plasmonic super absorbers," Nat. Commun. **2**, 517 (2011).
15. Y. Cui, K. H. Fung, J. Xu, H. Ma, Y. Jin, S. He, and N. X. Fang, "Ultrabroadband Light Absorption by a Sawtooth Anisotropic Metamaterial Slab," Nano Lett. **12**(3), 1443–1447 (2012).
16. H. Hu, D. Ji, X. Zeng, K. Liu, and Q. Gan, "Rainbow Trapping in Hyperbolic Metamaterial Waveguide," Sci Rep **3**, 1249 (2013).
17. L. Cao, P. Fan, A. P. Vasudev, J. S. White, Z. Yu, W. Cai, J. A. Schuller, S. Fan, and M. L. Brongersma, "Semiconductor Nanowire Optical Antenna Solar Absorbers," Nano Lett. **10**(2), 439–445 (2010).
18. L. Verslegers, Z. Yu, P. B. Catrysse, and S. Fan, "Temporal coupled-mode theory for resonant apertures," J. Opt. Soc. Am. B **27**(10), 1947 (2010).
19. M. Jablan, H. Buljan, and M. Soljačić, "Plasmonics in graphene at infrared frequencies," Phys. Rev. B **80**(24), 245435 (2009).
20. Z. Fang, S. Thongrattanasiri, A. Schlather, Z. Liu, L. Ma, Y. Wang, P. M. Ajayan, P. Nordlander, N. J. Halas, and F. J. García de Abajo, "Gated Tunability and Hybridization of Localized Plasmons in Nanostructured Graphene," ACS Nano **7**(3), 2388–2395 (2013).
21. A. Vakil and N. Engheta, "Transformation Optics Using Graphene," Science **332**(6035), 1291–1294 (2011).
22. G. W. Hanson, "Dyadic Green's functions and guided surface waves for a surface conductivity model of graphene," J. Appl. Phys. **103**(6), 064302 (2008).
23. S. Yi, M. Zhou, Z. Wang, and Z. Yu, "Superradiant absorption in multiple optical nanoresonators," Phys. Rev. B **89**(19), 195449 (2014).
24. S. Thongrattanasiri and F. J. García de Abajo, "Optical Field Enhancement by Strong Plasmon Interaction in Graphene Nanostructures," Phys. Rev. Lett. **110**(18), 187401 (2013).
25. Z. Fang, Y. Wang, A. E. Schlather, Z. Liu, P. M. Ajayan, F. J. García de Abajo, P. Nordlander, X. Zhu, and N. J. Halas, "Active Tunable Absorption Enhancement with Graphene Nanodisk Arrays," Nano Lett. **14**(1), 299–304 (2014).
26. Z. Yu, A. Raman, and S. Fan, "Fundamental limit of light trapping in grating structures," Opt. Express **18**(S3 Suppl 3), A366–A380 (2010).
27. J. J. Sakurai and J. J. Napolitano, *Modern Quantum Mechanics*, 2 edition (Addison-Wesley, 2010).
28. H. S. Song, S. L. Li, H. Miyazaki, S. Sato, K. Hayashi, A. Yamada, N. Yokoyama, and K. Tsukagoshi, "Origin of the relatively low transport mobility of graphene grown through chemical vapor deposition," Sci Rep **2**, 337 (2012).

1. Introduction

Emerging two-dimensional (2D) materials such as graphene have promising potentials for optoelectronic applications because of their unique electronic band structures and low dimensionality, which allows ultra-fast injection and extraction of charge carriers, enabling efficient energy conversion between electrons and photons [1–3]. However, their ultrathin feature limits the amount of time for photons interacting with the materials, resulting in an overall weak light-material interaction. For instance, the absorptance of a single layer of graphene is approximately 2.3% [4], which is impressive considering that it is absorbed by a single layer of atoms. But it is still too low to be useful for efficient optoelectronic devices. The light-material interaction must be significantly enhanced in order for 2D materials to achieve device efficiencies that are comparable to those based on conventional thick semiconductors.

Optical resonance has been employed as an effective means for enhancing the light-material interaction in conventional optoelectronic devices. There has been a great amount of recent interest in applying resonant enhancement in 2D materials. Existing methods can be divided into two categories. The first relies on conventional dielectric materials to construct optical resonators, such as Fabry-Perot cavities based on distributed Bragg reflectors [5] and guided resonances in photonic-crystal slabs [6, 7]. These approaches generally require sophisticated nanofabrication. The second category is based on the intrinsic plasmonic resonances. For instance, nanostructured graphene such as nano disks and ribbons support localized plasmonic resonances [8–10], particularly in the mid and far infrared spectral regimes. Such resonators do not require any additional dielectric material. Moreover, their resonant properties can be easily tuned by changing the geometrical shape. In both methods, 100% light absorption has been shown by operating the resonators at the critical coupling condition [6, 11].

#234896 - $15.00 USD Received 18 Feb 2015; revised 6 Apr 2015; accepted 8 Apr 2015; published 10 Apr 2015

However, there has been one significant challenge existing in both aforementioned methods in that the efficient light absorption can only be achieved in a narrow spectral range, which is limited by the bandwidth of a single type of resonator. For instance, the full width at half maximum (FWHM) of the perfect absorption reported in [11] is only about 6% of the resonant frequency. To overcome the bandwidth limitation, we design a multi-resonator approach based on plasmonic resonances of graphene. Compared to their resonant wavelengths, these graphene resonators have extremely small sizes, allowing multiple resonators with different frequencies to be densely packed in space. Each type of resonators is responsible for the enhancement of light-matter interaction in a limited bandwidth. Together, they offer an efficient broadband light absorption in a single layer of graphene. These closely packed deep-subwavelength resonators create an ultrathin medium with a high optical density of states [12–16], which enables broadband light absorption. The broadband absorption demonstrated here is one important step toward efficient 2D-material optoelectronic devices.

2. General strategy

Figure 1 illustrates the concept of broadband light absorption based on multiple resonators. A large area is covered by arrays of nanoresonators. These nanoresonators could be constructed by for example, a nanodisk of single-layer graphene. We use absorption cross-section σ_a to characterize the absorption of individual nanoresonators. σ_a is conceptually illustrated by the dashed circles in Fig. 1(a). Light falling within the circle is fully absorbed by the resonator. For efficient absorption over a large area, the dashed circles have to fill the most part of the space as shown in Fig. 1(a), which can be achieved if σ_a is larger than the geometrical size σ_g of the resonator. Arrays of the same type of resonators as in Fig. 1(a) have been used to achieve efficient absorption with resonators made from high-index semiconductors [17] and single-layer graphene [11]. Since the absorption cross-section decreases significantly away from the resonant frequency, only narrow-band absorption can be achieved in this way.

In order to broaden the spectral bandwidth, one has to rely on multiple resonators with different resonant frequencies [12]. Then a significant challenge arises because of the limited space to accommodate different types of resonators. To illustrate this point, we show three closely packed nanoresonators of different frequencies in Fig. 1(b). Their absorption cross-sections are coded with different colors to represent different resonant frequencies.

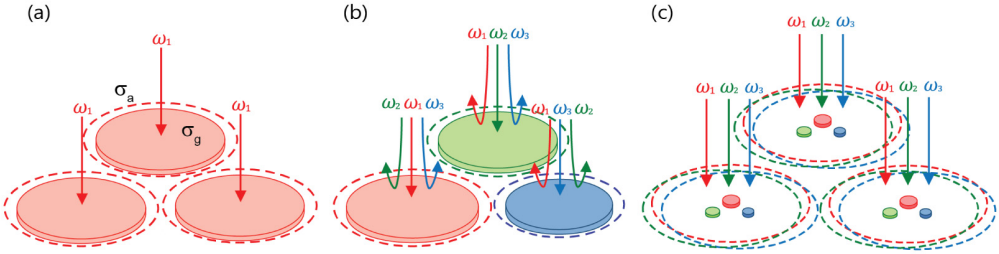

Fig. 1. Schematic of absorption cross-section (dashed line). Solid color disks represent the geometrical size of the nanoresonators. (a) Arrays of a single type of resonator with an absorption cross-section slightly larger than the geometrical size. Since the absorption cross-section can fill the space, efficient large-area absorption can be achieved for a single frequency of ω_1. (b) Arrays of three types of resonators with different resonant frequencies. The absorption is inefficient because the absorption cross-sections of different frequencies cannot cover the entire space. (c) Resonators with much smaller geometrical sizes enable efficient broadband absorption. Due to their small geometrical sizes, resonators can be closely packed so that the absorption cross-sections at different frequencies can all cover the entire space.

When the geometrical sizes σ_g are only slightly smaller than σ_a, the dashed circle of each color can only fill a subset of the space. Consequently, light absorption becomes less efficient when the bandwidth is broadened by multiple resonators. On the other hand, if σ_g

#234896 - $15.00 USD Received 18 Feb 2015; revised 6 Apr 2015; accepted 8 Apr 2015; published 10 Apr 2015

can be significantly smaller than the σ_a as shown in Fig. 1(c), one can place resonators closely with each other with their absorption cross-sections overlapping in space. When packed in arrays, dashed circles of each color can fill the space, resulting in efficient absorption in a broader spectral range. Base on this analysis, it is evident that the key to achieve broadband absorption is to realize a large σ_a / σ_g ratio.

To evaluate the ratio σ_a / σ_g, we can use a coupled mode theory [18] to derive the general form as

$$\sigma_a(\omega) = \frac{\lambda^2}{4\pi} \times \frac{\gamma_a \gamma_c}{(\omega - \omega_0)^2 + (\gamma_a + \gamma_c)^2 / 4} G \tag{1}$$

Where ω_o is the resonant frequency, λ is the resonant wavelength. γ_a and γ_c are the absorption and the coupling rate, respectively. γ_c represents radiation rate to the free space. It is percentage of energy stored in the resonator that is radiated to the free space per unit of time. Similarly, γ_a is the percentage of energy that is absorbed by the materials per unit of time. *G* is the directivity associated with the angular response of the resonator, which is 1 and 3/2 for isotropic and dipolar angular responses, respectively. To maximize σ_a, a resonator must operate at the critical coupling condition, i.e. $\gamma_a = \gamma_c$. In this case, the maximum absorption cross-section of an isotropic resonator ($G = 1$) is

$$\sigma_{a,\max} = \frac{\lambda^2}{4\pi} \tag{2}$$

which is obtained at the resonant frequency. Obviously, the maximal σ_a is only determined by wavelength.

On the other hand, the geometrical size σ_g is not necessarily related to σ_a. In most dielectric materials, σ_g scales as λ^2 / n^2 where *n* is the refractive index. Therefore the ratio of σ_a / σ_g is normally not a large number in the visible and infrared spectral ranges. However, in 2D materials that support plasmonic resonances, such as graphene, the geometrical size σ_g can be hundreds times smaller than the wavelength [19], leading to a unique opportunity to achieve a large σ_a / σ_g.

In addition to the requirement of a large ratio σ_a / σ_g, we also need analyze the near-field interaction among closely packed resonators. As we will show later, the near-field interaction introduces spectral competition of absorption cross-sections and often negatively impacts the absorption. The near-field interaction can be minimized by judiciously arranging the spatial configuration of nearby nanoresonators, the details of which will be discussed later.

3. Single graphene nanoresonators

Based on the general strategy outlined above, we now demonstrate a specific example based on graphene nanoresonators. Localized plasmonic resonances in graphene nanostructures exhibit extremely strong light confinement. The sizes of nanoresonators are often hundreds times smaller than the free-space wavelength [20]. Since σ_a is determined by the free-space wavelength, $\sigma_a / \sigma_g \gg 1$ can be realized.

We first calculate σ_a / σ_g of graphene nanoresonators by solving the full-wave Maxwell's equations numerically. We use a resonator with a square shape as shown in the inset of Fig. 2(a). It is placed on a perfect mirror with a dielectric spacer, which has a dielectric constant

#234896 - $15.00 USD Received 18 Feb 2015; revised 6 Apr 2015; accepted 8 Apr 2015; published 10 Apr 2015

$\varepsilon = 2.1$ and a thickness $t = 1.6\mu m$. Optical properties of graphene are modeled by the complex permittivity [21]

$$\varepsilon(\omega) = 1 + i\frac{\eta_s}{\varepsilon_0 \omega \Delta} \tag{3}$$

where $\Delta = 1nm$ is assumed for the thickness of graphene and η_s is the DC surface conductivity [22] given by

$$\eta_s = \frac{2e^2 k_B T}{\pi \hbar^2} \ln(2\cos h\frac{E_F}{2k_B T})\frac{i}{\omega + i\tau^{-1}} \tag{4}$$

with E_F being the chemical potential and τ the relaxation time. Here, only the intraband transition is considered and the interband transition is neglected because $\hbar\omega \ll E_F$ is satisfied in the frequency range of interest. The size of the graphene resonator is 100 nm × 100 nm and the doping level of graphene is assumed to be $E_F = 0.6eV$.

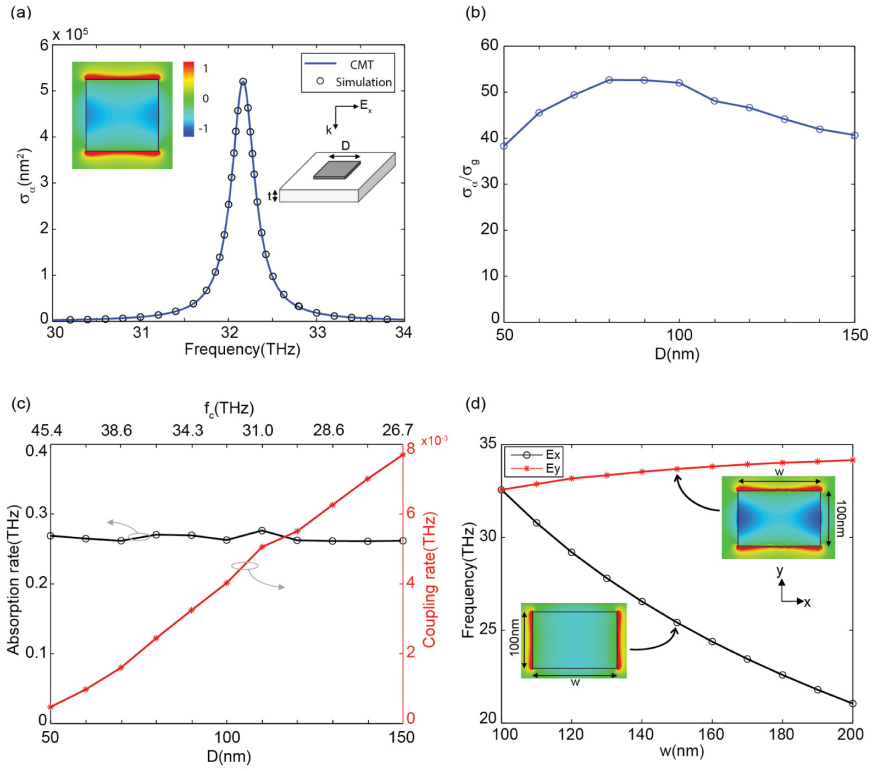

Fig. 2. (a) Absorption cross-section of a square graphene resonator with a size D = 100 nm. Dielectric constant of substrate is 2.1 and the thickness t = 1.6 μm. The simulation is performed with a periodic boundary condition with a very large period. The inset is the field distribution at the resonant frequency. Open circles are simulation and the solid line is coupled mode theory. (b) Ratio between the absorption cross-section (σ_a) and the geometric cross-section (σ_g) for different dimensions of graphene D. (c) Absorption rate and coupling rate as a function of graphene dimension D. (d) Resonant frequency shift with respect to graphene dimension. One side is fixed to 100nm, the other side w is varied from 100 nm to 200 nm. $E_{x(y)}$ represents the incident light in the x (y) polarization state.

The simulated absorption cross-section is shown in Fig. 2(a). The coupled mode theory shown in Eq. (1) agrees extremely well with the simulation result. The coupling and

#234896 - $15.00 USD Received 18 Feb 2015; revised 6 Apr 2015; accepted 8 Apr 2015; published 10 Apr 2015

absorption rates can easily be extracted from the fitted curve in Fig. 2(a). Most importantly, the resonant absorption cross-section of 5.2×10^5 nm^2 is more than 50 times larger than the geometrical size of 10^4 nm^2. Such a large ratio is not a result of any special choices of the shape or the size. In fact, we can see from Fig. 2(b) that the ratio stays around 40 for square sizes ranging from 50 nm to 100 nm. It is very difficult to achieve such a large ratio in conventional dielectric materials. For most dielectric materials, such as Si and Ge, σ_a is only slightly larger than σ_g [13]. Even though $\sigma_a > 40\sigma_g$, σ_a still does not reach the upper bound $\sigma_{a,\max}$ in Eq. (2). For a resonant wavelength of 9.32 um, the calculated $\sigma_{a,\max}$ is approximately 6.91 um^2, which is about 691 times of the geometrical size. The reason that this resonator does not reach the upper bound is because it operates in the under-coupling condition with $\gamma_c \ll \gamma_a$. Figure 2(c) shows the fitted absorption and coupling rates of these nanoresonators. It can be seen that $\gamma_c \le 0.03\gamma_a$. When the size increases, the coupling rate increases while the absorption rate remains about the same. To operate closer to the critical coupling condition, one could decrease the absorption rate by increasing the mobility of carriers in graphene.

To take advantage of the large ratio of σ_a / σ_g, we need a set of resonators of different frequencies, which can be easily achieved by tuning the shape of nanostructures. A graphene square supports two degenerate states that can be excited by x- or y- linearly polarized light. The degeneracy is lifted when one side of the square increases as shown in Fig. 2(d). The x-polarized resonance as in the lower inset of Fig. 2(d) shows a red shift as the size increases due to the first and also the dominant factor which is the length change along the polarization direction of the electric field. To the contrary, the y-polarized resonance as in the upper inset of Fig. 2(d) undergoes a blue shift. Since the length of the resonator in y-direction is fixed, changing length in x-direction does not affect the spatial length of the dipolar resonance. As a consequence, the second and the next dominant factor which is the perturbation effect [23] will take place and increase the resonant frequency due to negative dielectric constant of graphene.

4. Arrays of multiple graphene nanoresonators

So far, we have focused on the properties of individual nanoresonators. To obtain large-area light absorption, we need to use periodic arrays of graphene resonators. First, we discuss arrays that consist of a single type of resonator, which has been investigated in many previous works [11, 24, 25]. In contrast to these works, our focus here is to interpret the absorption based on the absorption cross-section.

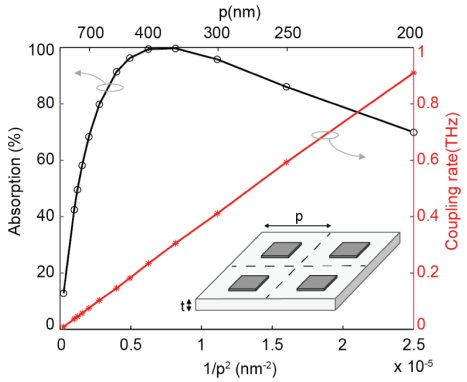

Fig. 3. Linear relationship between coupling rate and $1/p^2$ (red star). Period-dependent absorption (black circle) for arrays of graphene squares. The dimension of the square is 100 nm x 100 nm.

#234896 - $15.00 USD Received 18 Feb 2015; revised 6 Apr 2015; accepted 8 Apr 2015; published 10 Apr 2015

First, we show how the density of the nanoresonator affect the total large-area absorption by using an example of periodic arrays. The period p dictates the spatial density of resonators and thus how the absorption cross-sections fill the space. Figure 3 shows the simulated absorption of arrays of graphene squares. For very large periods, the absorption cross-sections (See dashed circles in Fig. 1) cannot fill the entire space and the large-area absorption is well below 100%. When p decreases, the large-area absorption increases because the absorption cross-sections can fill more of the space. 100% absorption is achieved when p is around 400 nm. It is interesting to note that the absorption does not increase monotonically with a decreasing p. We can use the coupled mode theory to understand such trend. Because of the presence of a back mirror and a period that is smaller than the wavelength, these resonators only radiate light into one direction [26]. As a result, one can calculate the large-area absorption as [6]

$$A = \frac{\gamma_c \gamma_a}{(\omega - \omega_0)^2 + (\gamma_c + \gamma_a)^2 / 4} \tag{5}$$

The absorption rate γ_a is again independent of the period and the shape of the resonator. On the other hand, the coupling rate γ_c scales linearly with $1/p^2$ as shown by the red line in Fig. 3. When $\gamma_c = \gamma_a$ at p ~400 nm, the critical coupling condition is satisfied and A = 100%. Further reducing the period increases γ_c and the resonator arrays enter the over-coupling condition $\gamma_c \geq \gamma_a$. The absorption then starts to decrease. The above analysis shows that overcrowded resonators in space actually reduces large-area absorption. This observation connects well with the effect of spectral competition to be discussed below.

For broadband absorption, we place multiple resonators of different frequencies in the unit cell. Ideally, each type of resonators can still absorb the same amount of light as the case when they are not placed together. However, the near-field interaction results in undesirable spectral competition. To quantify such competition, we define the spectral cross-section [14]

$$\rho = \int_0^\infty A(\omega) d\omega \tag{6}$$

It measures the total broadband absorption. Similar to the absorption cross-section σ_a, ρ has an upper limit that is determined by the number of types of resonator [14].

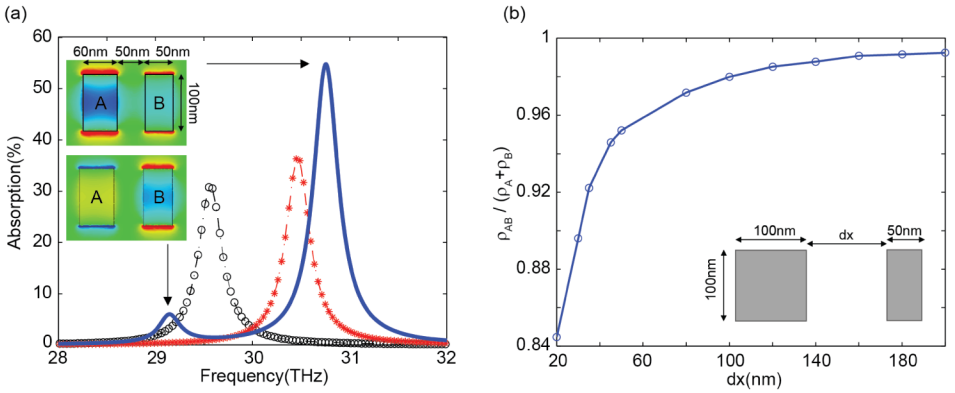

Fig. 4. (a) Absorption spectra for periodic arrays with only A-type resonator (stars), with only B-type resonator (circles), and with both A- and B-type resonators (solid line). Dot-dashed curves are based on coupled mode theory. (b) Ratio between total spectral cross-section (ρ_{AB}) and the upper bound of spectral cross-section ($\rho_A + \rho_B$) as the distance between two resonators dx increases from 20 nm to 200 nm.

#234896 - $15.00 USD Received 18 Feb 2015; revised 6 Apr 2015; accepted 8 Apr 2015; published 10 Apr 2015

We next use a specific example to illustrate the result of the spectral competition. We consider two types of resonators, A and B as shown in the inset of Fig. 4(a). Both are 100 nm long. Resonator A and B are 60 nm and 50 nm wide, respectively. The period is fixed at 850 nm. When the unit cell only has the A-type resonator, the absorption spectrum is shown by star markers (red) in Fig. 4(a). The case for B-type is shown by the circular markers (black). $\rho_{A(B)}$ can be easily calculated to measure the broadband absorption.

Now, we place both A- and B-type resonators together in the unit cell with a spacing of d = 50 nm between them. The absorption spectrum is shown by the solid blue line in Fig. 4(a). The spectral cross-section ρ_{AB} can also be calculated. It turns out that

$$\rho_{AB} \le \rho_A + \rho_B \tag{7}$$

because of the coupling between the two resonators. The coupling can be visualized by the field distribution at the two resonant peaks where the fields spread over two squares at both resonant frequencies as depicted in Fig. 4(a) insets. These two nanoresonators compete for the absorption, resulting in a total spectral cross-section ρ_{AB} that is smaller than the linear addition of ρ_A and ρ_B. The ratio $\rho_{AB}/(\rho_A+\rho_B)$ can be used to evaluate the spectral competition for different spatial configurations of the resonators. For example, Fig. 4(b) shows the ratio as a function of the spacing. It decreases when the spacing reduces, indicating greater spectral competition and more penalty in absorption. For large spacing, ρ_{AB} increases and $\rho_{AB}/(\rho_A+\rho_B)$ approaches 1. However, using large spacing to improve light absorption is a waste of the precious empty space between those resonators. These empty spaces are afforded by the deep sub-wavelength-sized resonators and should be used to fill more resonators with different frequencies to broaden the absorption bandwidth.

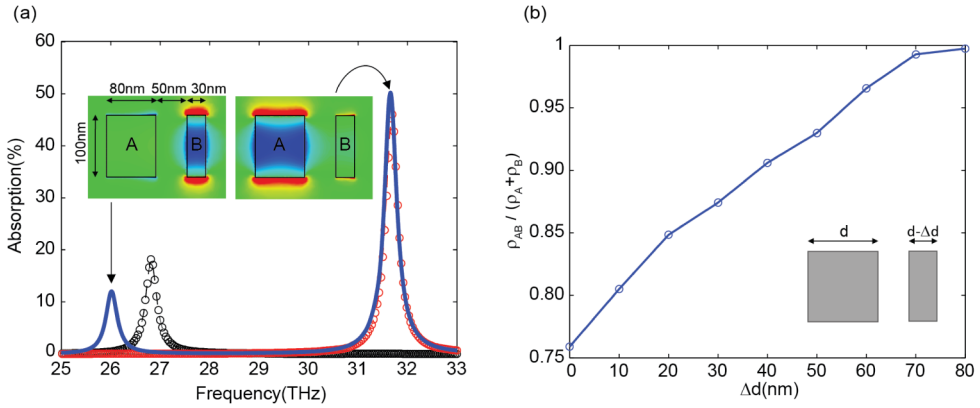

Fig. 5. (a) Absorption spectra for periodic arrays with only A-type resonator (red circles), with only B-type resonator (black circles), and with both A- and B-type resonators (solid line). Dashed curves are based on coupled mode theory. (b) Ratio between total spectral cross-section (ρ_{AB}) and the upper bound of spectral cross-section ($\rho_A+\rho_B$) as Δd varies from 0 nm to 80 nm. Distance between two graphene resonators is 50 nm.

To overcome this challenge, we use frequency detuning to suppress the spectral competition when the inter-resonant distance is small. As described in the perturbation theory [27], the effect of the coupling between resonant modes decreases when the difference between two resonant frequencies increases. To illustrate this point, we consider two graphene nanoresonators with quite different sizes. They are closely spaced in space, but their resonant frequencies are well separated. The spectral competition can be kept minimal. As shown in Fig. 5(a), the absorption spectrum (solid line) for the array consisting of both resonators is very close to the linear summation of the spectra of arrays that only consist of

#234896 - $15.00 USD Received 18 Feb 2015; revised 6 Apr 2015; accepted 8 Apr 2015; published 10 Apr 2015

individual resonators (markers). The field distributions in the inset of Fig. 5(a) at the two absorption peaks (blue line) also indicate that the nature of the resonances is dominated by that of individual resonators despite a small spacing of 50 nm. Figure 5(b) shows the ratio $\rho_{AB}/(\rho_A+\rho_B)$ as a function of the frequency detuning. The spacing is fixed at 50 nm. When the width difference between the two structures $\Delta d=0$, two resonators are identical. There is significant spectral competition and $\rho_{AB}/(\rho_A+\rho_B)=0.76$. When Δd increases, the frequency detuning increases and $\rho_{AB}/(\rho_A+\rho_B)$ approaches 1. Figure 5(b) shows that the general strategy of optimal spatial configuration is to place resonators of large frequency detuning closer and to keep resonators with similar frequencies far away.

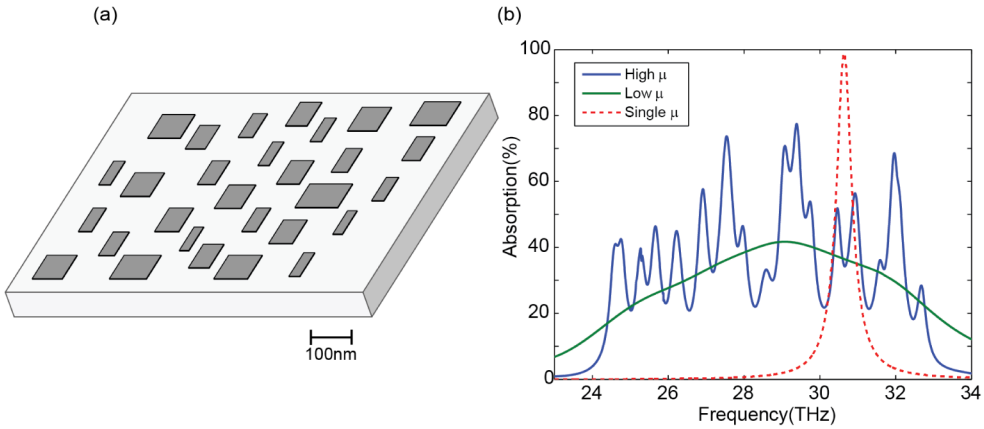

Fig. 6. (a) Layout of a broadband light absorber based on multiple graphene resonators. Period is 850nm, dielectric constant of the substrate is 2.1 and the thickness is 1.6 μm. (b) Absorption spectra of broadband light absorber in Fig. 6(a) with a mobility of 10,000 $cm^2V^{-1}s^{-1}$ (high μ) and 1,000 $cm^2V^{-1}s^{-1}$ (low μ). In comparison, dashed line shows the absorption by optimized arrays of single-type graphene resonator with limited bandwidth. A mobility of 10,000 $cm^2V^{-1}s^{-1}$ is used.

Following the strategy outlined above, we next show an example of broadband absorption in a single layer of graphene. The unit cell in Fig. 6(a) has 29 graphene resonators and the period is 850 nm. The sizes of these resonators are all deep sub-wavelength. There are 15 different types of resonators. The substrate is the same as used in Fig. 1. In particular, we place graphene resonators of similar sizes sparsely and resonators of different sizes closely. This arrangement is to reduce the spectral competition. Figure 6(b) shows the absorption spectrum, which exhibits broadband absorption spanning from 24 THz to 33 THz. The relative bandwidth $\Delta\omega/\omega_0$ is about 29%, where the central frequency $\omega_0=28.5$ THz. It consists of 17 resonant peaks, a number close to the number of types of the resonators. For comparison purpose, the dashed line in Fig. 6(b) shows the absorption of optimized arrays of a single type of resonators. The bandwidth is rather limited. In contrast, the multiple resonators approach significantly broadens the bandwidth. The total spectral absorption cross-section is enhanced by 4.6 times compared to the single resonator case. Here, we use a relatively high mobility for graphene μ = 10,000 $cm^2V^{-1}s^{-1}$. Higher mobility generally increases the light absorption because resonators can operate closer to the critical coupling condition. For experimental realization with graphene synthesized by chemical vapor deposition, the mobility is generally lower due to line defects originating from grain boundaries [28]. When mobility decrease, loss starts to increase and thus quality factor will decrease which leads to lower absorption peak and broader spectral width. In spite of low mobility, the broadband absorption enhancement can still be observed even when the mobility is only 1,000 $cm^2V^{-1}s^{-1}$ shown by solid curve (green) in Fig. 6(b).

#234896 - $15.00 USD Received 18 Feb 2015; revised 6 Apr 2015; accepted 8 Apr 2015; published 10 Apr 2015

5. Conclusion

In conclusion, we show a design based on multiple graphene nanoresonator to achieve broadband light absorption. There are two key factors. First, the absorption cross-section needs to be significantly larger than the geometrical size of the nanoresonators. This requirement ensures that many resonators can be packed together such that their absorption cross-sections at different frequencies can all fill the space. Graphene nanoresonators are particularly attractive in that the sizes of graphene resonators can be in the deep sub-wavelength regime with a very high ratio between the absorption cross-section and the geometrical size. Second, we need to arrange the spatial configuration of resonators to suppress spectral competition. For this purpose, a resonator should be neighbored by resonators with different frequencies. Again, graphene nanoresonators afford great tunability through changing the geometrical size. By fulfilling these two requirements, we show one example of broadband graphene absorber with an averaged absorption above 20% with a relative bandwidth of 29%, significantly higher than that of arrays of a single type of resonators. This method can also be applied to other deep sub-wavelength nanoresonators to enhance broadband light-matter interaction in ultrathin materials.

Acknowledgments

Z. Y acknowledges the financial support from the Office of Naval Research (grant number N00014-14-1-0300). J.Z. acknowledges support from the 973 Program (Grant Nos. 2013CB632701 and 2011CB922004) and the NSFC.

#234896 - $15.00 USD Received 18 Feb 2015; revised 6 Apr 2015; accepted 8 Apr 2015; published 10 Apr 2015